Title

Structural Insights into the Interaction between a Potent Anti-inflammatory Protein, Viral CC Chemokine Inhibitor (vCCI), and the Human CC Chemokine, Eotaxin-1*

Journal

Journal of Biological Chemistry, 289(10)

ISSN

0021-9258

Authors

Kuo, Nai-Wei

Gao, Yong-Guang

Schill, Megan S

et al.

Publication Date

2014-03-01

DOI

10.1074/jbc.m113.538991

THE JOURNAL OF BIOLOGICAL CHEMISTRY VOL. 289, NO. 10, pp. 6592–6603, March 7, 2014

Structural Insights into the Interaction between a Potent Anti-inflammatory Protein, Viral CC Chemokine Inhibitor (vCCI), and the Human CC Chemokine, Eotaxin-1*

Received for publication, November 28, 2013, and in revised form, January 28, 2014 Published, JBC Papers in Press, January 30, 2014, DOI 10.1074/jbc.M113.538991

Nai-Wei Kuo[‡], Yong-Guang Gao[§], Megan S. Schill[‡], Nancy Isern[¶], Cynthia M. Dupureur[‖], and Patricia J. LiWang[‡1]

From the [‡]Molecular Cell Biology, University of California, Merced, California 95343, the [§]Institute of Biochemistry and Cell Biology, Shanghai Institutes for Biological Sciences, Chinese Academy of Sciences, Shanghai 200031, China, the [¶]High Field NMR Facility, William R. Wiley Environmental Molecular Sciences Laboratory, Richland, Washington 99352, and the [‖]Department of Chemistry and Biochemistry, University of Missouri, St. Louis, Missouri 63121

Background: The mechanism used by viral protein vCCI to tightly bind to many CC chemokines is not known.
Results: Specific positively charged residues in the chemokine eotaxin-1 mediate binding to vCCI.
Conclusion: Basic residues in the chemokine each provide incremental affinity for vCCI.
Significance: This work shows how vCCI can bind a variety of CC chemokines.

Chemokines play important roles in the immune system, not only recruiting leukocytes to the site of infection and inflammation but also guiding cell homing and cell development. The soluble poxvirus-encoded protein viral CC chemokine inhibitor (vCCI), a CC chemokine inhibitor, can bind to human CC chemokines tightly to impair the host immune defense. This protein has no known homologs in eukaryotes and may represent a potent method to stop inflammation. Previously, our structure of the vCCI·MIP-1β (macrophage inflammatory protein-1β) complex indicated that vCCI uses negatively charged residues in β-sheet II to interact with positively charged residues in the MIP-1β N terminus, 20s region and 40s loop. However, the interactions between vCCI and other CC chemokines have not yet been fully explored. Here, we used NMR and fluorescence anisotropy to study the interaction between vCCI and eotaxin-1 (CCL11), a CC chemokine that is an important factor in the asthma response. NMR results reveal that the binding pattern is very similar to the vCCI·MIP-1β complex and suggest that electrostatic interactions provide a major contribution to binding. Fluorescence anisotropy results on variants of eotaxin-1 further confirm the critical roles of the charged residues in eotaxin-1. In addition, the binding affinity between vCCI and other wild type CC chemokines, MCP-1 (monocyte chemoattractant protein-1), MIP-1β, and RANTES (regulated on activation normal T cell expressed and secreted), were determined as 1.1, 1.2, and 0.22 nM, respectively. To our knowledge, this is the first work quantitatively measuring the binding affinity between vCCI and multiple CC chemokines.

Chemokines belong to a family of small (8–14-kDa) secreted proteins whose major function is to guide the migration and development of leukocytes. As such, chemokines play a major role in inflammation (1, 2). Despite differences in primary sequence and varied functions within the superfamily, chemokines all adopt very similar tertiary structures, including an extended N terminus followed by a globular core composed of a three-stranded β-sheet arranged in a Greek key motif with a C-terminal α-helix (3, 4). Traditionally, chemokines are divided into four subfamilies, C, CC, CXC, and CX3C, based on the arrangement of their N-terminal cysteine residues (5).

Due to their involvement in immune cell trafficking, chemokines have been implicated in a variety of inflammatory diseases, including rheumatoid arthritis, heart disease, asthma, type II diabetes, and cancer (6–10). In addition, chemokines have been implicated in the damaging activation and migration of immune cells in the brain after traumatic brain injury (11, 12). Therefore, the development of strategies to inhibit chemokine action has many potential benefits for human health.

Poxviruses and herpes viruses encode proteins that interfere with the actions of chemokines, probably facilitating viral evasion of the host immune system (13, 14). Three classes of such proteins have been identified: chemokine homologs, chemokine receptor homologs, and chemokine-binding proteins (15). For example, vMIP-II, a viral chemokine homolog encoded by human herpesvirus 8, broadly binds as an antagonist to CCR1, CCR2, CCR5, and CXCR4 (16) and binds as an agonist to CCR3 (17, 18) and CCR8 (19). On the other hand, US28, a chemokine receptor homolog encoded by the human cytomegalovirus, binds several human CC chemokines, including MCP-1(CCL2),[2] MCP-3(CCL7), MIP-1α(CCL3), MIP-1β(CCL4) and RANTES(CCL5), and the CX_3C chemokine, fractalkine, with high affinity and has shown the ability to sequester chemokines (20, 21). As for chemokine-binding proteins, poxviruses encode a protein called vCCI (viral CC chemokine inhibitor; also called "35K" due to its original presumed molecular weight). This type II chemokine-binding protein inhibitor

* This work was supported by United States Army Grant W911NF-11-1-0139.
[1] To whom correspondence should be addressed: Dept. of Molecular Cell Biology, University of California, 5200 N. Lake Rd., Merced, CA 95343. Tel.: 209-228-4568; E-mail: pliwang@ucmerced.edu.

[2] The abbreviations used are: MCP, monocyte chemoattractant protein; MIP, macrophage inflammatory protein; RANTES, regulated on activation normal T cell expressed and secreted; vCCI, viral CC chemokine inhibitor; HSQC, heteronuclear single quantum coherence; SUMO, small ubiquitin-like modifier; TROSY, transverse relaxation optimized spectroscopy.

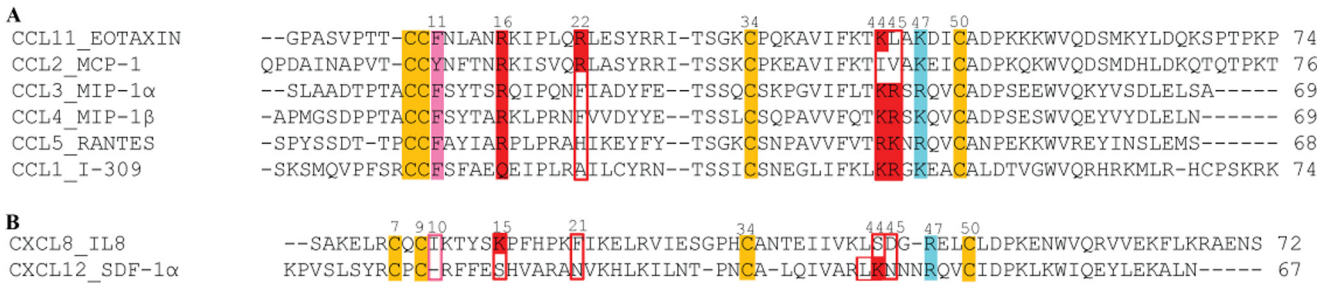

FIGURE 1. **Sequence comparison of CC chemokines (eotaxin, MCP-1, MIP-1α, MIP-1β, RANTES, and I-309) (*A*) and CXC chemokines (IL-8 and SDF-1α) (*B*).** Conserved cysteine residues are highlighted in *yellow*. The positively charged residues putatively critical to vCCI binding are highlighted in *red*. The hydrophobic residue putatively important in vCCI binding is highlighted in *pink*. The 47th position has been shown to modulate binding such that mutation to Ala can enhance binding to vCCI (*cyan*). In *A*, all of the chemokines are high affinity ligands for vCCI except for I-309 (for comparison, see Ref. 24). The sequence numbers in *A* are according to eotaxin, and those in *B* are according to IL-8.

binds to CC chemokines tightly and has been shown to potently inhibit the action of numerous CC chemokines *in vitro* and *in vivo*, making it an effective anti-inflammatory agent (13, 22–25) but raising the question of how one protein is able to bind with high affinity to more than 20 different proteins. vCCI has been shown to alleviate inflammation in the airway and the lung parenchyma (22) and may be relevant to respiratory diseases, such as asthma. Asthma involves an influx of inflammatory cells, including eosinophils, that respond to signaling, which is effected by the chemokine eotaxin family, eotaxin-1 (CCL11), eotaxin-2 (CCL24), and eotaxin-3 (CCL26) (26, 27).

Structural information has been presented for various chemokine binding proteins (28–37). The structure of vCCI from human cowpox virus was shown by x-ray crystallography to be composed of two parallel β-sheets, two short α-helices, and loops that connect the β-sheets and helices (28). One helix is on the edge of the structure, and the other short helix is in the exposed side of β-sheet I. A similar protein, EVM1 from mousepox, was also determined (33). A solution structure of rabbitpox vCCI in complex with a variant of human MIP-1β was also reported by us and showed the interaction surface of vCCI to be the β-sheet II side of the protein (32). The vCCI-chemokine interaction appears to be largely driven by the negatively charged surface of vCCI interacting with the positively charged regions of the chemokine. Critical residues on vCCI appeared to be negative charges at 141 and 143 and in the long loop region from 53 to 77. These residues interact with several conserved positive charges in the chemokine, including residue 18 and at least one residue at 24 or 45/46 of the 40s loop (the numbering is according to the MIP-1β sequence) (32). These chemokine positions have also been shown by mutagenesis of other chemokines to be important in vCCI binding (23, 38). More recently, mutagenesis has confirmed the essential role of vCCI residues Glu-143 and Tyr-80 in chemokine inhibition. This work also showed that the mutation of R89A in vCCI results in an increase in chemokine inhibition (25).

In the present work, we sought to expand our knowledge of vCCI interactions by studying this protein structurally and biochemically in complex with a chemokine having a different function than MIP-1β, namely eotaxin-1 (which will hereafter be referred to as eotaxin). Eotaxin has 36% sequence identity to MIP-1β (Fig. 1), but its receptor binding profile is quite different. Eotaxin is an important CC chemokine that has been shown to exist primarily as a monomer in many different buffer conditions, including pH 7.0 (39). This protein plays important roles in allergy and asthma pathogenesis (40). vCCI has been shown to be able to bind eotaxin and has also been shown *in vivo* to reduce airway inflammation, probably due at least in part to its ability to bind eotaxin (22). Whereas MIP-1β binds to the receptor CCR5 and mediates chemotaxis of macrophages and monocytes, eotaxin binds to CCR3 and mediates eosinophil influx, with particular relevance to asthma (41, 42). Therefore, a study of the vCCI-eotaxin interaction is particularly valuable for both biochemical insight and possible applications of medical importance. Here we use nuclear magnetic resonance (NMR) to determine the chemical shift assignments of the vCCI·eotaxin complex and use the docking program HADDOCK to model the interaction surface for the complex (43, 44). We have made mutations to putative critical residues on eotaxin and carried out binding experiments to vCCI using a fluorescence anisotropy binding assay that may be generally useful for studying vCCI interactions.

This work has allowed the identification of the contact surfaces present on vCCI and human eotaxin that are required for high affinity interaction with each other. The structural model of the vCCI·eotaxin complex is in agreement with the result from the fluorescence anisotropy binding data and indicates that vCCI binds to eotaxin similarly to MIP-1β, utilizing key residues of the chemokine. This work suggests the basis for the ability of vCCI to bind with high affinity to a broad array of chemokines.

EXPERIMENTAL PROCEDURES

Protein Expression and Purification—The encoding sequence for eotaxin and mutants was amplified via PCR and was cloned into the pET-28a(+) vector with a SUMO fusion tag (Novagen, Madison, WI). The plasmid was transformed into *Escherichia coli* BL21 (DE3) (Novagen, Madison, WI). Cells were grown at 37 °C. When A_{600} reached ~0.8, protein expression was induced by adding isopropyl β-D-1-thiogalactopyranoside to a final concentration of 1 mM. The culture was then shaken for 16 h at 16 °C, and the cells were harvested by centrifugation at 6000 × *g* for 10 min. The cell pellet was resuspended in 20 mM Tris, 500 mM NaCl, and 20 mM imidazole (pH 8.0) with 5 mM benzamidine and French pressed twice at 16,000 p.s.i. After centrifugation for 1 h at 27,000 × *g*, the supernatant was purified through a nickel-nitrilotriacetic acid column (GE Healthcare), and then the purified protein was dialyzed against

20 mM Tris and 50 mM NaCl, pH 7.0, buffer overnight at 4 °C for 16 h. During the dialysis, 60–80 μl of 100 μM Ulp1 protease (45) was added in the dialysis bag to cleave the SUMO fusion partner. After dialysis, precipitated matter was removed by centrifugation at 27,000 × *g* for 30 min. Finally, the cleaved protein was purified over a C4 reversed phase chromatography column (Vydac, Hesperia, CA) using the Akta purification system (GE Healthcare). Most SUMO tag precipitated out during dialysis. Protein concentration was quantified by measuring the absorbance at 280 nm. The chemokine MCP-1 was also prepared as described above. ^{15}N-Labeled and $^{2}H/^{15}N$-labeled protein was prepared by using M9 minimal medium containing $^{15}NH_4Cl$ (Cambridge Isotope Laboratory, Andover, MA) and/or D-[$^{13}C_6$]-glucose (Sigma-Aldrich) as the sole nitrogen and/or carbon resource, respectively. For deuterated samples for NMR, the medium was prepared with 95% (final concentration) D_2O.

MIP-1β-K45A/R46A/K48A, MIP-1β, and RANTES were amplified via PCR and were cloned into pET-28a(+) vector with a SUMO fusion tag. The purification of these proteins involved refolding, as described previously (46).

The gene encoding rabbitpox virus vCCI was cloned into pPIC9K plasmid and then transformed into *Pichia pastoris* strain SMD1168 (Invitrogen). Unlabeled, ^{15}N-labeled, $^{2}H/^{15}N$-labeled, and $^{2}H/^{13}C/^{15}N$-labeled protein samples were prepared as described previously (32).

NMR Spectroscopy—Spectra were recorded on a Bruker 600-MHz AVANCE III spectrometer equipped with a TCI cryoprobe at 37 °C. 2,2-Dimethyl-2-silapentane-5-sulfonic acid was used as an internal standard. Spectroscopic data were also collected on the vCCI·eotaxin complex at the High Field NMR Facility, William R. Wiley Environmental Molecular Sciences Laboratory, allowing initial chemical shift assignments and sample conditions to be tested. These experiments were carried out on Varian Inova 800 spectrometers (Varian, Palo Alto, CA). The NMRPipe software suite (47) was applied to process the NMR data. PIPP, NMRView (48), Sparky (49), and Mars (50) were used for visualization, resonance peak picking, and data analysis.

For $^{2}H/^{15}N/^{13}C$-labeled eotaxin and the $^{2}H/^{15}N/^{13}C$-labeled eotaxin/unlabeled vCCI complex, samples containing ~450 μM protein in a phosphate buffer (20 mM potassium phosphate, 100 mM NaCl, pH 7.0, and 0.05% (w/v) sodium azide in 95% H_2O, 5% D_2O) was used for NMR experiments. The backbone resonances were assigned based on the TROSY version of three-dimensional CBCA(CO)NH (51), HNCACB (51), HNCA (52), HN(CO)CA (51), HNCO (53), and HN(CA)CO (53).

For the $^{2}H/^{15}N/^{13}C$-labeled vCCI·unlabeled eotaxin complex, an NMR sample containing ~500 μM protein in phosphate buffer (20 mM potassium phosphate, 100 mM NaCl, pH 7.0, and 0.05% (w/v) sodium azide in 95% H_2O, 5% D_2O) was used for NMR experiments. The backbone resonances were assigned based on the TROSY version of three-dimensional HNCA, HN(CO)CA, CBCA(CO)NH, HNCACB, HNCO, and HN(CA)CO. The spectral overlay of the TROSY version of the vCCI·eotaxin complex compared with the HSQC of free vCCI (non-TROSY) (Fig. 2*A*) was made by correcting the chemical shift of the TROSY version of the vCCI·eotaxin complex by subtracting 0.76861 ppm in ^{15}N and adding 0.07789 ppm in ^{1}H as suggested by Tjandra *et al.* (54).

All two-dimensional HSQC experiments for unbound eotaxin variants and other CC chemokines were carried out at 25 °C with 50 μM protein in 20 mM potassium phosphate and 100 mM NaCl, pH 7, except for RANTES and MIP-1β, which were measured at 50 μM protein concentration in 20 mM potassium phosphate, pH 2.5 (data not shown). The HSQC spectra clearly show that the proteins are well folded except for eotaxin R16A/R22A/K44A, which has some peaks suggesting the presence of partially unfolded protein. HSQC experiments were run with carrier positions of 4.75 ppm for ^{1}H and 119.3 ppm for ^{15}N, sweep widths of 9615.385 Hz (15.9 ppm) for ^{1}H and 1938.672 Hz (31.8 ppm) for ^{15}N with 672 complex points in ^{1}H and 128 complex points in ^{15}N.

The weighted average chemical shift change of the ^{1}H and ^{15}N resonances for each residue upon binding was calculated using the following equation (55),

$$\Delta\delta_{obs} = \sqrt{\frac{\Delta\delta_H^2 + \left(\frac{\Delta\delta_N}{5}\right)^2}{2}} \qquad \text{(Eq. 1)}$$

where $\Delta\delta_H$ and $\Delta\delta_N$ are the chemical shift changes of the ^{1}H and ^{15}N dimensions, respectively. Here, the $\Delta\delta_{obs}$ is the difference between the bound and free forms of the ^{15}N-labeled complex.

Labeling Eotaxin-K63C with Fluorescein-5-maleimide—Eotaxin-K63C powder was dissolved in a buffer system composed of 20 mM potassium phosphate and 50 mM NaCl, pH 8.0. The concentration of eotaxin-K63C was adjusted to 50–100 μM. In the labeling reaction, 100–200 μM tris(2-carboxyethyl)phosphine (Thermo Fisher Scientific Inc., Waltham, MA) was added to reduce the disulfide bond potentially formed by K63C. The concentration of tris(2-carboxyethyl)phosphine is usually 2-fold higher than the eotaxin-K63C concentration. The mixture was first incubated at room temperature for 30 min to break up potential disulfide formation between two eotaxin-K63C monomers. Then fluorescein-5-maleimide powder (>10-fold concentration of eotaxin-K63C) was added into the solution (Anaspec, Inc., Fremont, CA). The labeling solution was incubated at 4 °C for 16 h. To remove excess fluorescein-5-maleimide and unlabeled eotaxin, two purification techniques were utilized. The first was a desalting column (GE Healthcare) to remove the unreacted fluorescein-5-maleimide. The second purification step utilized a C4 reversed phase column to separate fluorescein-labeled eotaxin-K63C from unlabeled eotaxin-K63C. The singly fluorescein-labeled eotaxin-K63C was confirmed by 17% SDS-PAGE (data not shown) and mass spectrometry (data not shown). Fluorescein-labeled eotaxin-K63C concentration was quantified by the Coomassie (Bradford) Protein Assay Kit (Thermo Scientific Pierce).

Fluorescence Anisotropy—All fluorescence anisotropy experiments were carried out with a PC1 spectrofluorimeter and VINCI software (ISS, Champaign, IL) at 25 °C controlled by a water bath (VWR International, Visalia, CA). The excitation and emission wavelength are 497 and 524 nm, respectively. All of the experiments were performed in 20 mM potassium phos-

phate and 100 mM NaCl, pH 7.0. For direct binding, 2 ml of 0.8 nM fluorescein-labeled eotaxin-K63C was used for each point. Different amounts of vCCI were mixed with fluorescein-labeled eotaxin-K63C, and measurements were taken until the anisotropy reached a plateau. The reaction was incubated at 25 °C for 5 min before measurement. All of the anisotropy values were normalized with respect to 1 as 100% bound. The data were fit to a system of mass conservation equations and the following,

$$\theta = \frac{[L]_{free} \times K_a}{1 + [L]_{free} \times K_a} \quad \text{(Eq. 2)}$$

where θ is the fraction of eotaxin bound, $[L]_{free}$ is the free vCCI concentration, and K_a is the association constant. Fitting the data in this way using Scientist software (version 2.02, Micromath, St. Louis, MO) means that it is not necessary to approximate $[L]_{free}$ with $[L]_{total}$. Each reported K_d value ($1/K_a$) is an average of three independent experiments.

For competition binding, an 8 nM concentration of a 1:1 ratio vCCI·eotaxin complex was prepared. 500 μl of the complex was mixed with different amounts of unlabeled eotaxin mutant and incubated at 25 °C for 30 min to ensure that the competition binding reached equilibrium. The measurements with different amounts of unlabeled mutants were taken until no additional change in anisotropy was observed. All of the anisotropy values were normalized with respect to 1 as 100% bound. The resulting data were fit to a system of equations describing both the vCCI·eotaxin-fluor equilibrium (known K_d) and the respective unlabeled eotaxin-variant equilibrium (unknown K_d) using Scientist software (Micromath, Salt Lake City, UT) as described previously (58, 59).

Docking—Modeling of the vCCI·eotaxin complex was performed using the HADDOCK docking program (version 2.1) (43, 44, 56), with both mutagenesis data and fluorescence anisotropy data providing information for restraints. The starting structures for the docking were the NMR structures of vCCI (Protein Data Bank code 2FFK) and eotaxin (Protein Data Bank code 1EOT). The active and passive residues for HADDOCK were based on the chemical shift perturbation data observed for eotaxin and vCCI upon complex formation, competition fluorescence anisotropy studies of eotaxin variants, and vCCI mutagenesis data (25) and solvent accessibility as calculated by VADAR (57). Active residues were defined as having a chemical shift perturbation upon complex formation greater than 0.165 ppm for vCCI and 0.21 ppm for eotaxin with an average relative solvent accessibility higher than 40%. All amino acids neighboring the active residues with a high solvent accessibility (>40%) and oriented toward the interaction interface were defined as passive residues. A 2-Å distance was used to define the ambiguous interaction restraints. During the rigid body energy minimization, 1000 structures were calculated. The 200 best solutions were followed by a refinement in explicit water. Finally, the structure with the best HADDOCK score was ranked first.

RESULTS

Mapping the Contact Surface between vCCI and Eotaxin—To obtain detailed insight into the molecular interface between vCCI and eotaxin, NMR titration and chemical shift assignments of vCCI in the presence of eotaxin-1 were carried out at 37 °C and pH 7.0). Fig. 2*A* shows the HSQC spectra of ^{15}N-labeled vCCI in the presence and absence of eotaxin. NMR titrations that were performed with ^{15}N-labeled vCCI and unlabeled eotaxin at 37 °C and pH 7.0 caused noticeable changes of many peaks in the spectrum, indicating specific interaction between these two proteins. The fully liganded spectrum is shown in *red* in Fig. 2*A*, and a residue by residue histogram of chemical shift changes is shown in Fig. 2*C*. Residues exhibiting significant chemical shift changes (above 1 S.D. from the average: 0.165 ppm) were mapped onto the structure of the vCCI (Fig. 2*E*). The significantly perturbed residues (chemical shift changes above 1 S.D. greater than average) are located in the β-strand 2 (Thr-49 and Ile-51), β-strand 3 (Thr-78, Thr-79, Tyr-80, and Ser-82), β-strand 4 (Asn-91, Phe-94, and Thr-95), β-strand 7 (Val-144 and Ser-145), β-strand 8 (Phe-195), β-strand 9 (Lys-216), in the flexible region between β-strand 2 and β-strand 3 (Thr-52 and Glu-53), and in the loop region after β-strand 5 (Lys-96) (Fig. 2*E*). All of the perturbed residues form a distinct patch on the β-sheet II surface of vCCI (Fig. 2*E*). For comparison, the HSQC spectrum and chemical shift changes upon MIP-1β addition to ^{15}N-labeled vCCI are shown in Fig. 2, *B* and *D*, respectively. The assignments of vCCI·MIP-1β are from our previous work (30–32). Residues of vCCI exhibiting significant chemical shift changes (above 0.107 ppm) upon the addition of MIP-1β were mapped onto the structure of the vCCI (Fig. 2*F*). The significantly perturbed residues also formed a distinct patch on the β-sheet II surface of vCCI, which is very similar to the surface induced by the addition of eotaxin. Upon eotaxin or MIP-1β binding, vCCI also reveals significant chemical shift changes in the loop between β2 and β3 strands and a few additional changes across the β-sandwich in β-sheet I (Fig. 2, *C* and *D*).

Chemical shift assignments and NMR titrations were also carried out with a "reverse" labeling scheme (*i.e.* with ^{15}N-labeled eotaxin and unlabeled vCCI at 37 °C and pH 7.0). The addition of unlabeled vCCI into ^{15}N-labeled eotaxin resulted in noticeable changes of many peaks in the HSQC spectrum (Fig. 3*A*), again indicating specific interaction between these two proteins. The residue by residue chemical shift changes are shown in Fig. 3*B*, and the residues exhibiting significant chemical shift changes (above the average shift of 0.21 ppm) were mapped onto the structure of eotaxin (Fig. 3*C*). The significantly perturbed residues are located in the N-loop (Cys-10, Phe-11, Asn-12, Leu-13, and Arg-16) and Cys-50. The 20s loop (Leu-20, Gln-21, Leu-23), 40s loop (Thr-43), and other residues, including Ala-38 and Asp-48, also have chemical shift changes above the average of chemical shift change upon vCCI binding. The majority of changes are located in the N-loop of the chemokine, which is also a surface used in the CC chemokine dimer interface. This suggests that binding by vCCI occurs at or near the chemokine dimer interface and probably interferes with chemokine dimer formation. Similar changes were observed in the same interface upon MIP-1β binding to vCCI (32). Overall, these chemical shift perturbations indicate that both eotaxin and MIP-1β bind vCCI similarly.

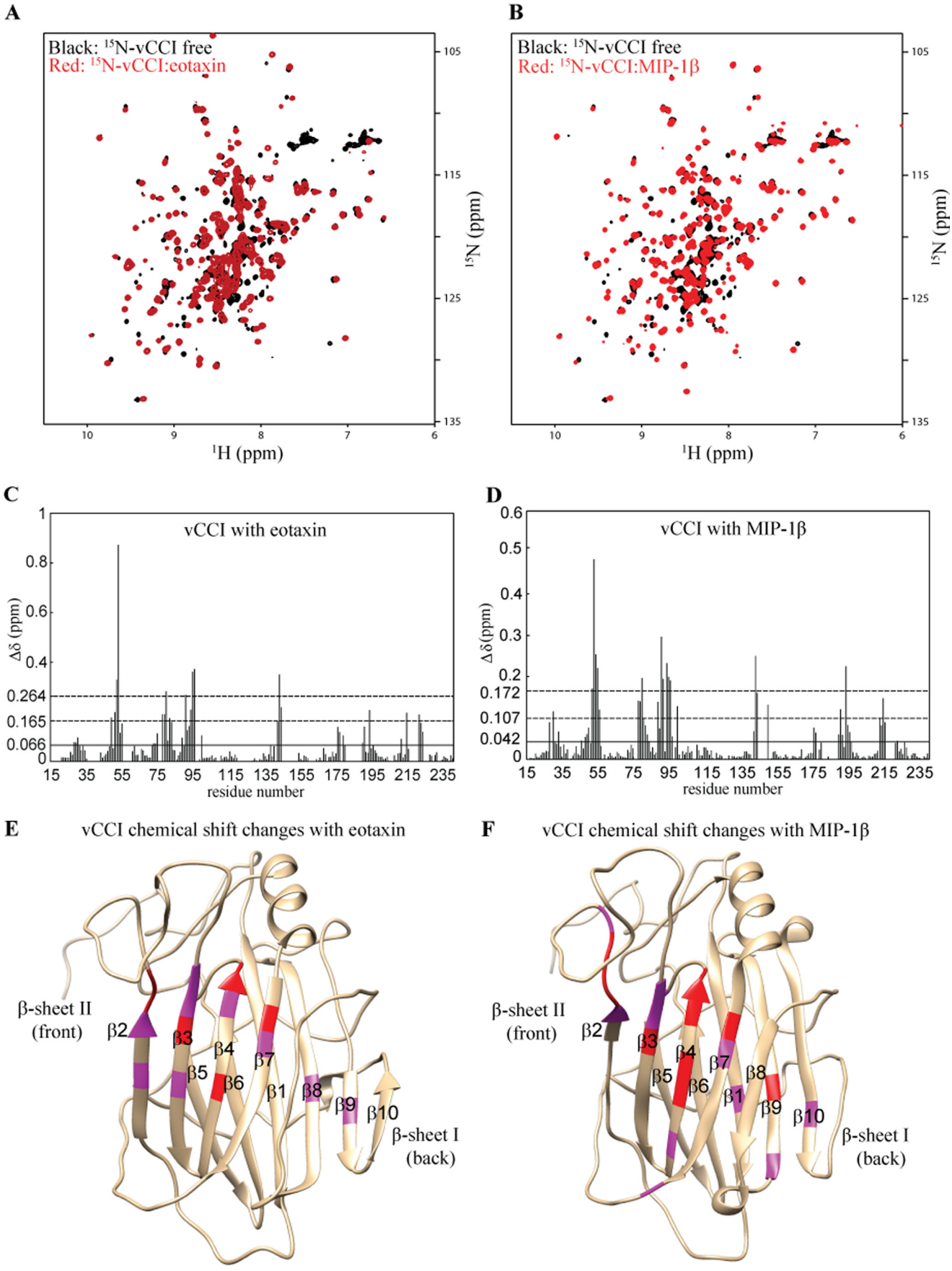
A
Black: ^{15}N-vCCI free
Red: ^{15}N-vCCI:eotaxin
^{15}N (ppm)
^{1}H (ppm)
B
Black: ^{15}N-vCCI free
Red: ^{15}N-vCCI:MIP-1β
^{15}N (ppm)
^{1}H (ppm)
C
vCCI with eotaxin
Δδ (ppm)
residue number
D
vCCI with MIP-1β
Δδ(ppm)
residue number
E
vCCI chemical shift changes with eotaxin
β-sheet II
(front)
β-sheet I
(back)
F
vCCI chemical shift changes with MIP-1β
β-sheet II
(front)
β-sheet I
(back)

Eotaxin Binds vCCI with High Affinity—To understand the binding properties of vCCI and eotaxin, we made mutants based on the vCCI·MIP-1β structure (32) and performed binding studies using fluorescence anisotropy. Binding interactions appear to derive from hydrophobic interaction of Phe-13 and electrostatic interaction of Arg-18 and residues 24/45/46 on MIP-1β to the corresponding region of vCCI. Therefore, to obtain direct evidence for those specific interactions between vCCI and eotaxin, these eotaxin variants, including single point mutations, double point mutations, and triple point mutations, at these residues were constructed and purified to determine their importance for binding. All of the mutants and their binding affinities are shown in Table 1.

To carry out fluorescence anisotropy studies, a fluorescent probe, fluorescein-5-maleimide, was linked to eotaxin via a cysteine on eotaxin resulting from a K63C mutation. Lys-63 is located at the second turn of the C-terminal α-helix, which is distal from the vCCI interaction surface and is solvent-exposed. Mass spectroscopy results confirmed (data not shown) the fluorescein-labeled eotaxin-K63C (hereafter referred to as eotaxin-fluor) is singly labeled. To determine the ability of eotaxin-fluor to bind vCCI, 0.8 nM eotaxin-fluor was titrated with increasing concentrations of vCCI (Fig. 4*A*, *left*). The anisotropy changes indicated that complex formation increased with increasing vCCI concentration until saturation, as expected. The value of K_d for vCCI·eotaxin was calculated to be 0.65 $\pm$ 0.17 nM. This value was used to fit all of the mutants and other CC chemokines in the competition binding assays that will be described below. As a control to show that this modified eotaxin-fluor has essentially wild type binding, a competition experiment was carried out in which 8 nM eotaxin-fluor and vCCI (1:1 ratio; 10-fold above K_d) were preincubated and then mixed with different amounts of unlabeled wild type eotaxin. The decreasing anisotropy observed (Fig. 4*A*, *right*) indicates that non-fluorescently labeled wild type eotaxin successfully competes with the eotaxin-fluor. The K_d of the vCCI-eotaxin interaction from this control competition was calculated to be 0.29 $\pm$ 0.12 nM. The successful competition between eotaxin-fluor and unlabeled eotaxin with vCCI indicates that eotaxin-fluor is functional and can be useful in competition assays to determine the ability of variant eotaxin and other chemokines to bind vCCI.

Electrostatic Interactions Are Important for Eotaxin and vCCI Binding—The charged residue Arg-16 (eotaxin numbering) is conserved among most CC chemokines, including MCP-1, MIP-1α, MIP-1β, and RANTES (Fig. 1*A*). In addition, the charged residues located in the 20s and 40s loops of CC chemokines have been suggested to be important for contributing to the interactions between chemokines and vCCI (23, 32, 38). Based on the structural information from the vCCI·MIP-1β complex, Arg-16 of eotaxin is in close proximity to the negatively charged Asp-141 and Asp-143 of vCCI (32). This residue was mutated in eotaxin, and the R16A variant gave a K_d of 3.1 $\pm$ 0.61 nM, representing a 4.8-fold reduction in affinity for vCCI, in competition experiments against vCCI·eotaxin-fluor (Fig. 4*B*). Residue 24 and residues 45 and 46 in the 40s loop of MIP-1β are close to the acidic loop of vCCI (32). Single-site mutations in the analogous resides of eotaxin (Arg-22 and Lys-44, corresponding to residues 24 and 45 in MIP-1β) were made, and the proteins were produced and purified. Competition fluorescence anisotropy studies were performed with these variants. Eotaxin R22A and K44A mutants showed a K_d with vCCI of 1.3 $\pm$ 0.57 and 0.97 $\pm$ 0.34 nM, respectively, indicating only an affinity loss of about 2- and 1.5-fold (Fig. 4*B*). This unexpectedly small loss of binding affinity suggests the possibility that there may be compensation for the loss of only one of the two proximal basic residues because the other site (position 22 or 44) was still positively charged. This is consistent with the suggestion from our work with the vCCI·MIP-1β complex that positively charged residues in the 40s loop compensate for residues in the 20s loop, because those groups are proximal (32). Therefore, in addition to single point mutants, we also made the double point mutant, R22A/K44A. Another double point mutant, R16A/R22A, and triple point mutant, R16A/R22A/K44A, were also made to determine the importance of the overall electrostatic interaction by removing more charged residues from this surface. The K_d of R22A/K44A was 3.1 $\pm$ 0.93 nM, showing a more robust 4.8-fold decrease in affinity and suggesting that these two residues may compensate for each other, with a loss of affinity occurring only if both are neutralized, whereas high affinity is retained if only one charge is removed. The other double mutant, R16A/R22A, resulted in a K_d of 12 $\pm$ 2.2 nM, an 18-fold decrease in affinity. The triple mutant, R16A/R22A/K44A, represents a loss of a basic residue at the spatially isolated 16th position as well as removal of charge at the co-localized 22/44 positions. This results in a K_d of 87 $\pm$ 29 nM, showing a 134-fold decrease in affinity. These results suggest that charged residues at positions 16 and 22/44 are both important and that, regarding 22/44, a single basic residue at 22 or 44 can compensate for the lack of charge at the other position due to the proximity of these two residues.

To further investigate electrostatic interaction between vCCI and eotaxin, we also made reverse-charged mutants, R22E and R16A/R22E, in which positively charged Arg-22 was mutated to negatively charged Glu (Fig. 4*B*). Both mutants showed much lower affinity with vCCI than the positive-to-neutral variants, with K_d values of 22 $\pm$ 2.5 nM (34-fold decrease in affinity) and 27 $\pm$ 7.2 nM (42-fold decrease in affinity).

FIGURE 2. **Mapping the contact surface of eotaxin and MIP-1β on vCCI.** *A*, overlay of the ^{1}H-^{15}N HSQC spectra of free vCCI (*black*) and eotaxin-bound vCCI (*red*). In these spectra, only the vCCI is isotopically labeled with ^{15}N. *B*, overlay of the ^{1}H-^{15}N HSQC spectra of free vCCI (*black*) and MIP-1β-bound vCCI (*red*). *C*, chemical shift changes of vCCI *versus* its residue number upon binding to eotaxin. ^{15}N-Labeled vCCI was combined with unlabeled eotaxin to a final molar ratio of 1:1. The average chemical shift change ($\Delta\delta$) is indicated with a *solid horizontal line*. The *dashed lines* indicate the 1 and 2 S.D. values from the average. Residues with chemical shift changes above 0.165 ppm (1 S.D.) are considered significantly involved in contact with eotaxin. *D*, as in *C*, except that ^{15}N-labeled vCCI was combined with unlabeled MIP-1β. Residues with the chemical shift changes above 0.107 ppm (1 S.D.) are considered significantly involved in contact with MIP-1β. *E*, mapping the significant eotaxin contact residues on the vCCI structure. *Pink*, chemical shift changes above 1 S.D. greater than average; *red*, chemical shift changes above 2 S.D. values greater than average. The vCCI structure is from cluster 1 of the docked structure. *F*, as in *E*, except mapping the significant MIP-1β contact residues on the vCCI structure (Protein Data Bank code for vCCI: 2FFK). *B*, *D*, and *F*, all MIP-1β data shown here are from Ref. 32 and used for comparison.

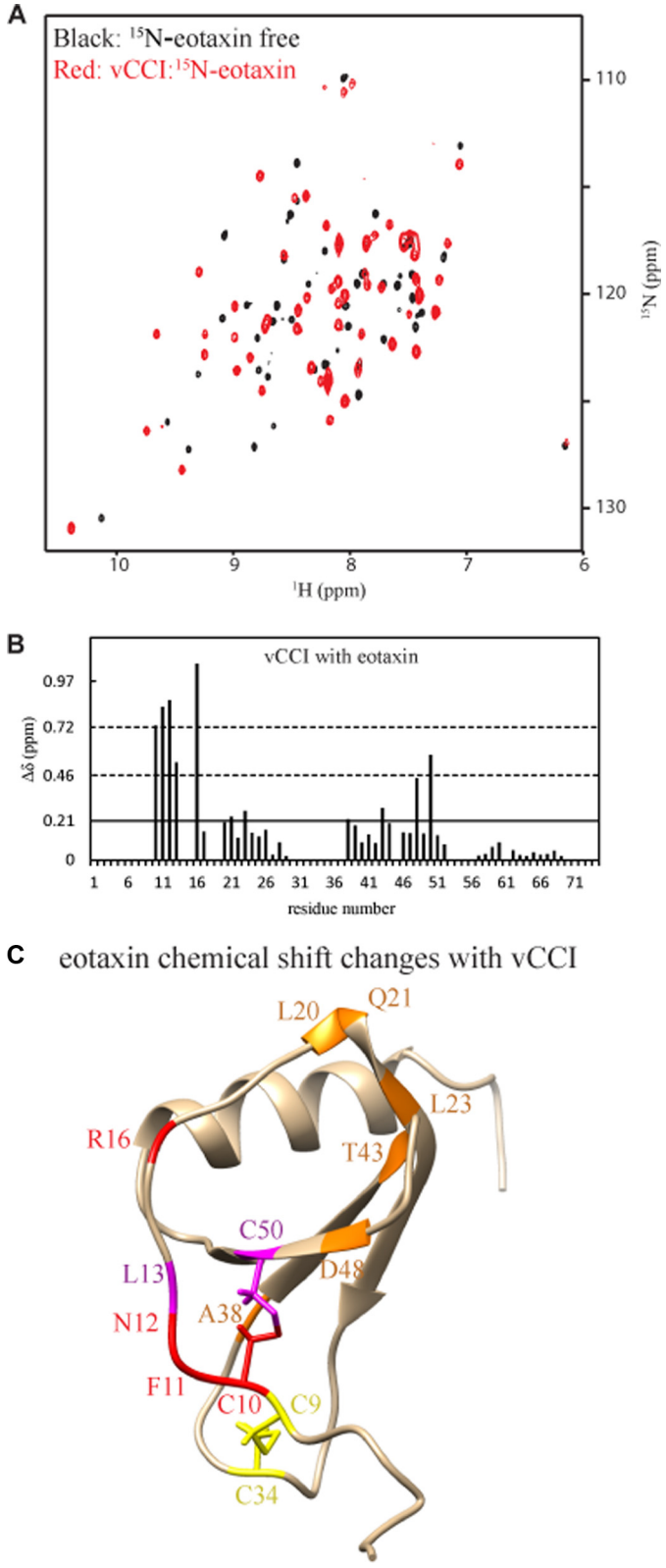

FIGURE 3. **Mapping the contact surface of vCCI on eotaxin.** *A*, overlay of the ^{1}H-^{15}N HSQC spectra of free ^{15}N eotaxin (*black*) and vCCI-bound ^{15}N eotaxin (*red*). *B*, chemical shift changes of eotaxin *versus* its residue number upon binding vCCI. ^{15}N-Labeled eotaxin was combined with unlabeled vCCI to a final molar ratio of 1:1. The average chemical shift change (Δδ) is indicated with a *solid horizontal line*. Residues with the chemical shift changes above 0.21 ppm are considered significantly involved in contact with vCCI. *C*, mapping the significant vCCI contact residues on the eotaxin structure. *Orange*, chemical shift changes above the average; *pink*, chemical shift changes above 1 S.D. greater than average; *red*, chemical shift changes above 2 S.D. values greater than average. *Yellow*, disulfide bond; the other disulfide bond is C10:C50. The eotaxin structure is from cluster 1 of the docked structure.

TABLE 1
Fluorescence anisotropy results of interaction between vCCI and eotaxin variants or between vCCI and other CC chemokines

Mutants	K_d	Change ($K_{d,\mathrm{mut}}/K_{d,\mathrm{WT}}$)[a]
	nM	*-fold*
WT eotaxin	0.65 ± 0.17	1.0
F11A	1.7 ± 0.47	2.6
R16A	3.1 ± 0.61	4.8
R22A	1.3 ± 0.57	2.0
R22E	22 ± 2.5	34
K44A	0.97 ± 0.34	1.5
K47A	0.08 ± 0.06	0.12
R16A/R22A	12 ± 2.2	18
R22A/K44A	3.1 ± 0.93	4.8
R16A/R22E	27 ± 7.2	42
R16A/R22A/K44A	87 ± 29	134
MCP-1	1.1 ± 0.11	1.7
MIP-1β	1.2 ± 0.17	1.8
MIP-1β-K45A/R46A/K48A	2.2 ± 0.36	3.4
RANTES	0.22 ± 0.087	0.34

[a] Comparison is with wild-type eotaxin. K_d values are calculated as described under "Experimental Procedures." Errors are the S.D., determined from three independent experiments. Student's *t* test to compare the K_d of each variant with the wild type protein resulted in a *p* value less than 0.05 for all variants except for F11A, R22A, and K44A, which each had a *p* value greater than 0.05.

The putative hydrophobic interaction mediated by Phe-11 on eotaxin was also investigated. In the vCCI·MIP-1β complex, this residue appears to be located within the binding distance to a hydrophobic pocket of vCCI (32). The Phe-11 of eotaxin was mutated to Ala, and the K_d of the F11A variant was determined to be 1.7 ± 0.47 nM (a 2.6-fold reduction in affinity), indicating that Phe-11 may have some contribution to the interaction with vCCI, which agrees with the previous finding that Tyr-13 in MCP-1 has an impact on binding vCCI (23, 38).

Interestingly, it has been reported that substitution of residue Lys-47 to Ala in MCP-1 actually results in an increased affinity for vCCI binding (23, 38), and it has been suggested based on the vCCI·MIP-1β structure that this might be due to relief of its steric crowding and poor electrostatic interaction between the Lys of the chemokine and nearby residues, Tyr-80 and Arg-89 on vCCI (32). Therefore, an eotaxin variant at the analogous location (K47A) was produced. The K_d of the interaction between vCCI and eotaxin K47A was determined to be 0.08 ± 0.06 nM (Fig. 4*B*), showing an 8-fold increase in affinity compared with wild type eotaxin, making the variant the tightest binding ligand of vCCI among eotaxin variants. This result suggests that this position is in close proximity to vCCI and that in this area of interaction, a small neutral amino acid on eotaxin is better for affinity than a basic residue.

vCCI Binds to Other Wild Type Chemokines—Although the qualitative binding capacity of vCCI to other CC chemokines has been established (24, 32), there is still a lack of quantitative information. vCCI binds most CC chemokines but not C, CXC, and CX3C chemokines (13, 24). To gain quantitative binding information for several CC chemokines and vCCI, we used competition fluorescence anisotropy to investigate the binding of vCCI by the CC chemokines, MCP-1, MIP-1β, and RANTES. These proteins have been shown to activate different receptors, including CCR1, CCR2, and CCR5. However, they all bind vCCI tightly (23, 24, 38). We also used the competition fluores-

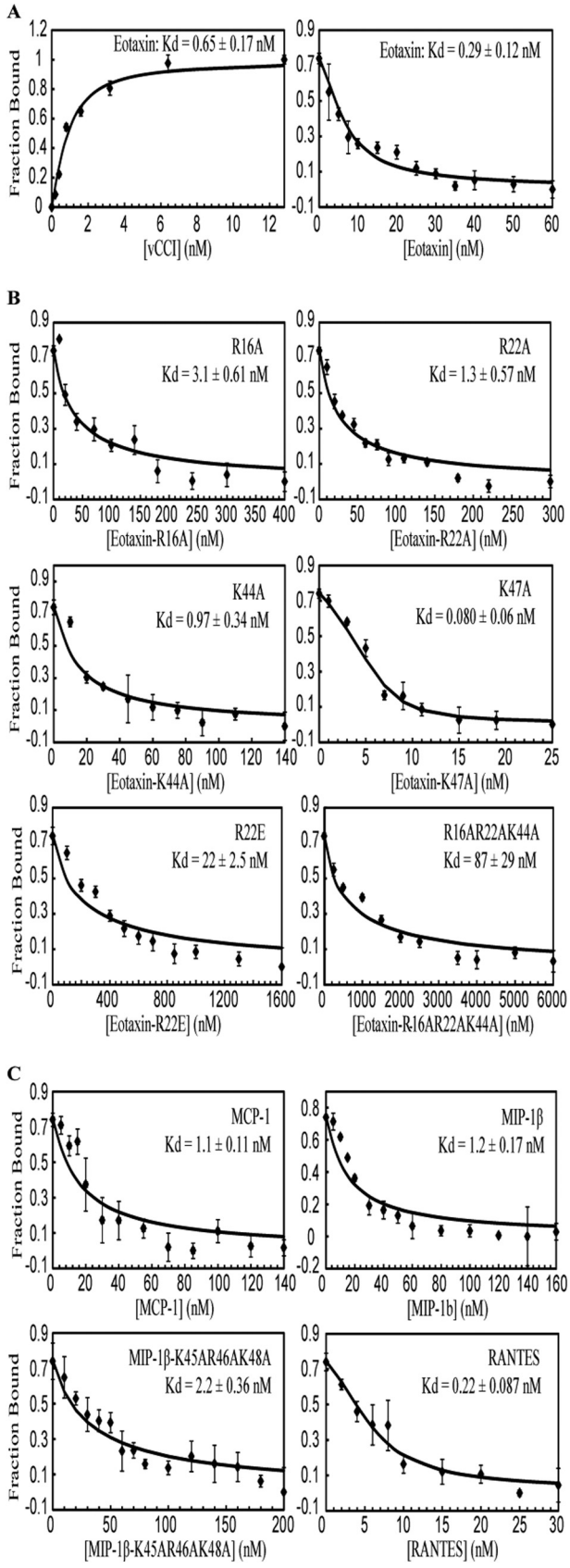

FIGURE 4. **Fluorescence anisotropy studies of binding of eotaxin, eotaxin variants, and other CC chemokines to vCCI.** *A*, *left*, fluorescence anisotropy of eotaxin-fluor binding to vCCI. *Right*, fluorescence anisotropy competition assay between unlabeled eotaxin and a complex of eotaxin-fluor and vCCI. *B*, selected fluorescence anisotropy competition assays between unlabeled eotaxin variants and a complex of eotaxin-fluor and vCCI. *C*, fluorescence anisotropy competition assays between unlabeled CC chemokines and a complex of eotaxin-fluor and vCCI. Three independent experiments were performed for each assay. The graphs show a representative experiment. *Error bar*, S.D. of multiple measurements of that point. The K_d was calculated as described under "Experimental Procedures."

cence assay to determine the affinity for vCCI of MIP-1β-K45A/R46A/K48A, the variant that was used as the basis for the vCCI·MIP-1β structure (32). The K_d values of these four chemokines as determined by fluorescence anisotropy are as follows: MCP-1, 1.1 ± 0.11 nM; MIP-1β, 1.2 ± 0.17 nM; MIP-1β-K45A/R46A/K48A, 2.2 ± 0.35 nM; and RANTES, 0.22 ± 0.087 nM. This is in agreement with previous work, although surface plasmon resonance studies with MCP-1 showed a higher affinity (0.29 nM (23) and 0.34 nM (38)).

Model of the vCCI·Eotaxin Complex—To gain structural insight into the binding interface between vCCI and eotaxin and the role of different residues in binding, docking of the complex was performed using the HADDOCK program (43, 44, 56). The residues chosen as "active" were required to fulfill the following three criteria: 1) chemical shift perturbation at that residue is larger than average upon binding and/or mutagenesis at the residue, resulting in significant changes in binding affinity in the fluorescence anisotropy assay; 2) the residue is >40% solvent-accessible; and 3) the side chains point outward to possibly form an interface rather than inward for self-interaction (56). Residues were chosen to be "passive" if they were neighboring residues of active residues, if they were 40% solvent-accessible, and if the side chain was generally directed toward the interaction interface rather than inward (56). For vCCI, recent mutagenesis data were also considered (25). For this protein, seven active (positions 53, 78, 80, 96, 143, 180, and 215) and four passive (positions 76, 89, 141, and 182) residues were selected. For eotaxin, five active (positions 12, 16, 22, 44, and 47) and four passive (positions 11, 22, 45, and 49) residues were selected. These residues were used to generate ambiguous interaction restraints between vCCI and eotaxin (2.0 Å cut-off). The 200 calculated structures after water refinement clustered in a total of eight groups. The average intermolecular energies of resulting clusters were between −711.1 and −420.1 kcal/mol, and average intermolecular root mean square deviations were between 1.4 and 11.3 Å. Cluster 1 (the cluster with the lowest energy and the best HADDOCK score) was the dominant cluster, containing 98 structures, with the lowest intermolecular energies of −711.1 kcal/mol and the lowest intermolecular root mean square deviations of 1.4 Å. Fig. 5*A* shows the overlay *ribbon representation* of the best scoring structure of this cluster. Fig. 5*B* shows an overlay of the *ribbon representation* of one structure from this cluster (*champagne*) and the vCCI·MIP-1β complex (*blue*; Protein Data Bank code 2FFK). Fig. 5, *C* and *D*, depict the interaction interface of vCCI and eotaxin, respectively. The average buried surface area of the 98 structures in cluster 1 is 1858.8 $Å^2$. The overall structure of the vCCI·eotaxin complex is similar to that of the vCCI·MIP-1β complex that was obtained by NMR restraints using the program Dynamo (Fig. 5*B*) (60). In the structure, β-sheet II of vCCI exhibits interactions with the N-loop, 20s region, 40s loop, and

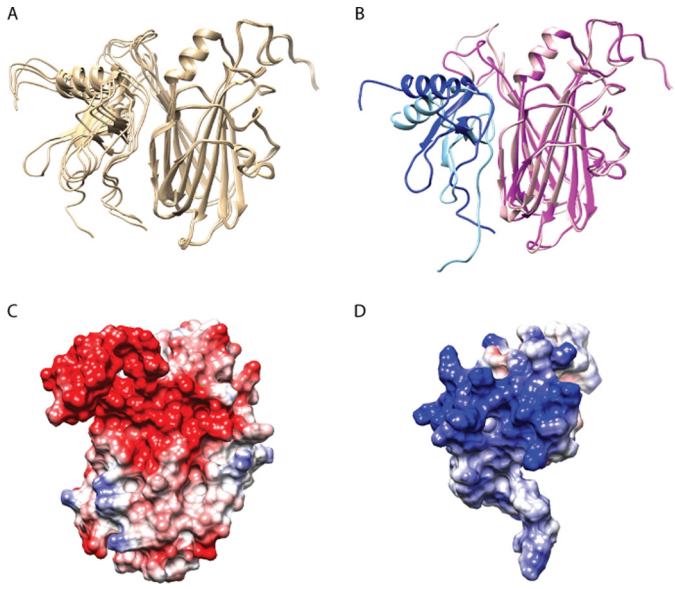

FIGURE 5. **Structural model of the vCCI·eotaxin complex.** *A*, overlay of four docking structures from the vCCI·eotaxin cluster 1. Eotaxin is shown on the *left*, and vCCI is shown on the *right*. *B*, overlay of the vCCI·eotaxin (*pink* and *blue*) complex and the vCCI·MIP-1β (*light pink* and *light blue*) complex for comparison. The vCCI·MIP-1β complex is from Ref. 32. *C* and *D*, electrostatic potential maps are shown for the binding interface of vCCI (*C*) and eotaxin (*D*). Negatively charged residues are shown in *red*, and positively charged residues are shown in *blue*. The vCCI and eotaxin surface is from cluster 1 of the docked structure.

the third β-strand of eotaxin. Some small differences were observed between the two structures, however, including the docked vCCI·eotaxin structure showing a longer β2 strand (Fig. 2*E*), the eotaxin showing some β-structure around residue 20 (Fig. 3*C*), and the overall tilt of the chemokine being somewhat different between eotaxin and MIP-1β (Fig. 5*B*). Some of these differences could be due to the lower resolution inherent in a docked structure.

DISCUSSION

vCCI is a secreted protein encoded by poxviruses that contributes to the evasion of the host immune response (61). vCCI can bind specifically and generically to CC chemokines with high affinity, making it a potent and specific anti-inflammatory agent with demonstrated effectiveness *in vivo* (22, 62). A comprehensive analysis of the binding profile of vCCI with an extensive panel of more than 80 chemokines revealed that vCCI binds to 26 CC chemokines with high affinity, including 14 human chemokines, such as eotaxin, MCP-1, MIP-1α, MIP-1β, and RANTES (24). Although vCCI possesses no close molecular similarity to known mammalian or other eukaryotic proteins (13, 63), its broad spectrum, high affinity CC chemokine binding ability suggests that it might provide further clues as to how to develop specific therapeutic agents to abrogate chemokine-mediated disease conditions.

The vCCI-Eotaxin Interaction—As shown in Fig. 4 and Table 1, our data show three residues in eotaxin that are potentially critical in binding vCCI: Arg-16, Arg-22, and Lys-44. Arg-16 of eotaxin is a relatively isolated and basic residue. When this residue is mutated, the variant R16A shows an almost 5-fold loss of binding to vCCI, making it the worst single point mutation among the alanine substitution mutants. This indicates that position 16 is important in the interaction with vCCI. In work using surface plasmon resonance with the chemokine MCP-1, the R18A variant in MCP-1 (in the corresponding position) caused a >20-fold reduction in affinity to vCCI (23, 38), and in general, high affinity vCCI-binding chemokines have a basic residue in this position (Fig. 1*A*). Electrostatic potential mapping of eotaxin in Fig. 5*D* clearly shows that this amino acid is located in a positively charged patch on the surface of eotaxin. When in complex with vCCI, this residue is close to the conserved, negatively charged vCCI residues Asp-141 and Glu-143, indicating its probable involvement in electrostatic interactions. In a recent study, both positions 141 and 143 of vCCI were mutated with charge swap residues or alanine, with the result that Asp-141 mutants impaired the function of the protein, and the Glu-143 charge swap mutant led to total loss of function (25).

Two residues in the chemokine that are also important for binding, Arg-22 and Lys-44, are spatially close to each other. These two amino acids are located in a highly positively charged patch that is very close to the loop in vCCI between the β2 and β3 strands. This loop region of vCCI is highly negatively charged, as shown in Figs. 2*E* and 5*C*, and is quite flexible (32), so it would be expected to interact favorably with positively charged residues in the chemokine. It was suggested by Zhang *et al.* (32) that at least one positive charge in the 22/44 position was required for high affinity binding to vCCI and that the absence at one position could be compensated for by the presence of a basic residue at the other (in that paper, the residue numberings were 24 and the adjacent 45/46 positions). The present work supports this prediction, because R22A, K44A, and R22A/K44A single and multiple mutants in eotaxin showed weaker binding, particularly when both residues were mutated. The suggestion that high affinity binding to vCCI requires a positive charge in the 22/44 position of the chemokine is also supported by previous work that showed that R24A in MCP-1 caused a >10-fold drop in affinity; in this chemokine, Arg-24 (position 22 in eotaxin) is the only cognate positive charge because there is no corresponding basic residue in the 44-position in MCP-1 (Fig. 1) (23). Therefore, loss of this positively charged amino acid cannot be compensated for by a nearby positive charge in MCP-1. The present experiments show that a single point mutation, R22A in eotaxin, caused only a 2-fold reduction in affinity for vCCI, whereas an R22E mutant caused 34-fold loss of binding, strongly indicating the role of electrostatic interactions at this site. This is consistent with work on MCP-1, where it was shown that the R24E mutation had no detectable binding to vCCI, indicating that a negatively charged amino acid is disfavored in this position (38). The chemokine MIP-1β possesses a hydrophobic amino acid (Phe-24; Fig. 1) in this position and still binds to vCCI with high affinity (32), indicating that a large hydrophobic residue is also tolerable here (and in the case of MIP-1β is probably compensated for by the basic residues in the 45/46 positions).

In the present structure model (Fig. 5), Arg-16 and some residues from the 40s loop in eotaxin are involved in the interaction with vCCI. The corresponding residues in MIP-1β are in its GAG-binding region (32, 64, 65), so it is possible that vCCI also

interferes with GAG binding by eotaxin. Interference with the chemokine concentration gradient formation through inhibiting its GAG binding capability may be a general strategy for a virus to escape or utilize the host immune response (66, 67).

The mutation F11A in eotaxin resulted in a 2.6-fold reduction in affinity for vCCI (Table 1). The equivalent residue in MIP-1β (Phe-13) makes close contact with a hydrophobic patch of vCCI at the edge of the two sheets of the vCCI β-sandwich (32). Mutation of an analogous residue, Y13A, in MCP-1 showed a ~10-fold reduction in affinity (23, 38). In all human chemokines that bind to vCCI with high affinity, a hydrophobic amino acid or an aromatic amino acid is located in this position (24). The conservation of this position in chemokines that bind vCCI with high affinity suggests the importance of this residue for them to bind the chemokine inhibitor vCCI. The analogous residue Phe-13 in MIP-1β has been shown to be critical for receptor binding and for dimer formation (68), and has been demonstrated to be critical for several other CC chemokines (69, 70), indicating that vCCI probably functions through competition for the binding of chemokines to its receptors.

The N-terminal region of CC chemokines is important for receptor binding and dimer formation (71), but this region is not likely to be important in binding to vCCI. In the present model of vCCI·eotaxin (Fig. 5), the N terminus of eotaxin is not involved in the interaction, but the model is not definitive because it is based on NMR data, which shows no peaks for this region, probably due to high flexibility in the chemokine here (Fig. 3). However, the flexibility that is implied by the lack of resonances in both forms indicates that the N terminus is not involved in binding to vCCI. Our results are consistent with other work showing that the N termini of MIP-1β and MCP-1 do not contribute to binding vCCI (23, 32, 38). This highlights one strategy used by vCCI to bind chemokines; vCCI probably does not contact regions of high flexibility and disparity but recognizes epitopes that are relatively rigid and conserved among the CC chemokines.

Rationale for vCCI Binding Interactions—The vCCI·eotaxin structure model presented here is very similar to the vCCI·MIP-1β complex structure (Fig. 5*B*) (32). This similarity is evident from the similar chemical shift changes exhibited by vCCI upon binding of MIP-1β or eotaxin, as shown in Fig. 2, and the docked structure from the current vCCI·eotaxin data shows great similarity to the NMR-derived structure of vCCI·MIP-1β (Fig. 5). It is interesting that vCCI binds to eotaxin in a similar way as it binds to MIP-1β despite the identity between the two proteins being only 36% and their general lack of ability to cross-react with each other's cognate receptor.

It has been shown qualitatively that vCCI binds to most CC chemokines well but does not bind CXC chemokines, such as SDF-1α and IL-8, although the monomeric tertiary structures of CC and CXC chemokines are highly similar. The main reason for this difference could be because the interaction between vCCI and its ligand CC chemokines derives mainly from electrostatic interaction at specific conserved positions, such as 16, 22, and 44/45 (according to eotaxin numbering). However, corresponding residues in CXC chemokines, such as SDF-1α and IL-8, possess mostly non-charged residues at these locations (Fig. 1). Whereas eotaxin has three basic residues in the key positions 16, 22, and 44/45, IL-8 and SDF-1α have only one positively charged residue (and a basic residue in the "unfavorable" position 47) (Fig. 1*B*). This lack of a properly positioned basic surface may explain why IL8 and SDF-1α bind more weakly to vCCI. Indeed, whereas CC chemokines with the positively charged residues at 16, 22, or 44/45 result in high affinity binding to vCCI (24), CC chemokines, such as I-309, possess a neutral Gln at position 16 and also tend to show weaker binding to vCCI (24). Our work suggests that this is due to the lack of a basic residue in this position. Unlike the 22/44-positions that are close in space to each other and can compensate for each other, Arg-16 is isolated. Because chemical shift perturbation in eotaxin shows significant changes in this position, it appears that this residue is involved in binding vCCI and is most effective when positively charged (Fig. 3*B*). Therefore, it could also explain why there is only slightly weaker binding of MIP-1β-K45A/R46A/K48A compared with wild type MIP-1β (Table 1) because this mutant retains a positive charge at position Arg-18. Overall, the data support the conclusion that electrostatic interaction is a major factor in the vCCI-CC chemokine interaction.

As mentioned, several techniques have been utilized in past and present studies to investigate the vCCI-chemokine interaction, leading to the overall consistent picture described here. Surface plasmon resonance has been used to investigate the binding of the chemokine MCP-1 with vCCI, and this work indicated a vCCI·MCP-1 binding K_d of 0.3 nM (23, 38). In the work by Zhang *et al.* (32), the EC_{50} for WT MIP-1β was found to be 0.66 nM using an ELISA-type assay. In the present work, fluorescence anisotropy indicates that eotaxin binds to vCCI with a K_d of 0.65 $\pm$ 0.17 nM. The results of a fluorescence competition binding assay also provide a vCCI·MCP-1 K_d of 1.09 $\pm$ 0.11 nM and a vCCI·MIP-1β K_d of 1.16 $\pm$ 0.17 nM. In addition, we show that RANTES, which also has appropriately placed basic residues, binds to vCCI the most tightly (K_d = 0.22 $\pm$ 0.087 nM), which is consistent with the importance of electrostatic interactions in vCCI binding. These methods each provide a consistent measure of the tight binding of chemokines to vCCI and are also consistent with the more qualitative work of Burns *et al.*, who studied an extensive list of wild type chemokines (24).

This eotaxin-binding pattern of vCCI modeled here shows a general strategy for vCCI to interfere with the immune system: effectively masking important residues in CC chemokines that are required for interaction with receptors or possibly cell surface GAGs. Overall, the data indicate that each basic residue in eotaxin has an incremental effect on vCCI binding, leading to overall high affinity. This suggests how each chemokine can have some combination of these "binding blocks" to also arrive at high affinity for vCCI without necessarily showing sequence identity with each other.

In summary, this work reveals a general strategy for vCCI to selectively bind to chemokines with high affinity, which will help facilitate the rational design of chemokine receptor antagonists. The studies have contributed to insight into the binding modes of these viral proteins and host chemokines.

Acknowledgments—We thank Dr. Yong-Gang Chang and Dr. Li Zhang. A portion of the research was performed using EMSL, a national scientific user facility sponsored by the Department of Energy's Office of Biological and Environmental Research and located at Pacific Northwest National Laboratory.

REFERENCES

1. Charo, I. F., and Ransohoff, R. M. (2006) The many roles of chemokines and chemokine receptors in inflammation. *N. Engl. J. Med.* **354,** 610–621
2. Rot, A., and von Andrian, U. H. (2004) Chemokines in innate and adaptive host defense. Basic chemokinese grammar for immune cells. *Annu. Rev. Immunol.* **22,** 891–928
3. Fernandez, E. J., and Lolis, E. (2002) Structure, function, and inhibition of chemokines. *Annu. Rev. Pharmacol. Toxicol.* **42,** 469–499
4. Lau, E. K., Allen, S., Hsu, A. R., and Handel, T. M. (2004) Chemokine-receptor interactions. GPCRs, glycosaminoglycans and viral chemokine binding proteins. *Adv. Protein Chem.* **68,** 351–391
5. Luster, A. D. (1998) Chemokines. Chemotactic cytokines that mediate inflammation. *N. Engl. J. Med.* **338,** 436–445
6. Kunkel, S. L., Lukacs, N., Kasama, T., and Strieter, R. M. (1996) The role of chemokines in inflammatory joint disease. *J. Leukoc. Biol.* **59,** 6–12
7. Terkeltaub, R., Boisvert, W. A., and Curtiss, L. K. (1998) Chemokines and atherosclerosis. *Curr. Opin. Lipidol.* **9,** 397–405
8. Acker, F. A., Voss, H. P., and Timmerman, H. (1996) Chemokines. Structure, receptors and functions. A new target for inflammation and asthma therapy? *Mediators Inflamm.* **5,** 393–416
9. Pickup, J. C. (2004) Inflammation and activated innate immunity in the pathogenesis of type 2 diabetes. *Diabetes Care* **27,** 813–823
10. Vicari, A. P., and Caux, C. (2002) Chemokines in cancer. *Cytokine Growth Factor Rev.* **13,** 143–154
11. Riva-Depaty, I., Fardeau, C., Mariani, J., Bouchaud, C., and Delhaye-Bouchaud, N. (1994) Contribution of peripheral macrophages and microglia to the cellular reaction after mechanical or neurotoxin-induced lesions of the rat brain. *Exp. Neurol.* **128,** 77–87
12. Woodcock, T., and Morganti-Kossmann, M. C. (2013) The role of markers of inflammation in traumatic brain injury. *Front. Neurol.* **4,** 18
13. Smith, C. A., Smith, T. D., Smolak, P. J., Friend, D., Hagen, H., Gerhart, M., Park, L., Pickup, D. J., Torrance, D., Mohler, K., Schooley, K., and Goodwin, R. G. (1997) Poxvirus genomes encode a secreted, soluble protein that preferentially inhibits β chemokine activity yet lacks sequence homology to known chemokine receptors. *Virology* **236,** 316–327
14. Graham, K. A., Lalani, A. S., Macen, J. L., Ness, T. L., Barry, M., Liu, L. Y., Lucas, A., Clark-Lewis, I., Moyer, R. W., and McFadden, G. (1997) The T1/35kDa family of poxvirus-secreted proteins bind chemokines and modulate leukocyte influx into virus-infected tissues. *Virology* **229,** 12–24
15. Lalani, A. S., and McFadden, G. (1999) Evasion and exploitation of chemokines by viruses. *Cytokine Growth Factor Rev.* **10,** 219–233
16. Kledal, T. N., Rosenkilde, M. M., Coulin, F., Simmons, G., Johnsen, A. H., Alouani, S., Power, C. A., Lüttichau, H. R., Gerstoft, J., Clapham, P. R., Clark-Lewis, I., Wells, T. N., and Schwartz, T. W. (1997) A broad-spectrum chemokine antagonist encoded by Kaposi's sarcoma-associated herpesvirus. *Science* **277,** 1656–1659
17. Boshoff, C., Endo, Y., Collins, P. D., Takeuchi, Y., Reeves, J. D., Schweickart, V. L., Siani, M. A., Sasaki, T., Williams, T. J., Gray, P. W., Moore, P. S., Chang, Y., and Weiss, R. A. (1997) Angiogenic and HIV-inhibitory functions of KSHV-encoded chemokines. *Science* **278,** 290–294
18. Weber, K. S., Gröne, H. J., Röcken, M., Klier, C., Gu, S., Wank, R., Proudfoot, A. E., Nelson, P. J., and Weber, C. (2001) Selective recruitment of Th2-type cells and evasion from a cytotoxic immune response mediated by viral macrophage inhibitory protein-II. *Eur. J. Immunol.* **31,** 2458–2466
19. Sozzani, S., Luini, W., Bianchi, G., Allavena, P., Wells, T. N., Napolitano, M., Bernardini, G., Vecchi, A., D'Ambrosio, D., Mazzeo, D., Sinigaglia, F., Santoni, A., Maggi, E., Romagnani, S., and Mantovani, A. (1998) The viral chemokine macrophage inflammatory protein-II is a selective Th2 chemoattractant. *Blood* **92,** 4036–4039
20. Kuhn, D. E., Beall, C. J., and Kolattukudy, P. E. (1995) The cytomegalovirus US28 protein binds multiple CC chemokines with high affinity. *Biochem. Biophys. Res. Commun.* **211,** 325–330
21. Kledal, T. N., Rosenkilde, M. M., and Schwartz, T. W. (1998) Selective recognition of the membrane-bound CX3C chemokine, fractalkine, by the human cytomegalovirus-encoded broad-spectrum receptor US28. *FEBS Lett.* **441,** 209–214
22. Dabbagh, K., Xiao, Y., Smith, C., Stepick-Biek, P., Kim, S. G., Lamm, W. J., Liggitt, D. H., and Lewis, D. B. (2000) Local blockade of allergic airway hyperreactivity and inflammation by the poxvirus-derived pan-CC-chemokine inhibitor vCCI. J. *Immunol.* **165,** 3418–3422
23. Beck, C. G., Studer, C., Zuber, J. F., Demange, B. J., Manning, U., and Urfer, R. (2001) The viral CC chemokine-binding protein vCCI inhibits monocyte chemoattractant protein-1 activity by masking its CCR2B-binding site. *J. Biol. Chem.* **276,** 43270–43276
24. Burns, J. M., Dairaghi, D. J., Deitz, M., Tsang, M., and Schall, T. J. (2002) Comprehensive mapping of poxvirus vCCI chemokine-binding protein. Expanded range of ligand interactions and unusual dissociation kinetics. *J. Biol. Chem.* **277,** 2785–2789
25. White, G. E., McNeill, E., Christou, I., Channon, K. M., and Greaves, D. R. (2011) Site-directed mutagenesis of the CC chemokine binding protein 35K-Fc reveals residues essential for activity and mutations that increase the potency of CC chemokine blockade. *Mol. Pharmacol.* **80,** 328–336
26. Zimmermann, N., Hershey, G. K., Foster, P. S., and Rothenberg, M. E. (2003) Chemokines in asthma. Cooperative interaction between chemokines and IL-13. *J. Allergy Clin. Immunol.* **111,** 227–242; quiz 243
27. Hogan, S. P. (2007) Recent advances in eosinophil biology. *Int. Arch. Allergy Immunol.* **143,** 3–14
28. Carfí, A., Smith, C. A., Smolak, P. J., McGrew, J., and Wiley, D. C. (1999) Structure of a soluble secreted chemokine inhibitor vCCI (p35) from cowpox virus. *Proc. Natl. Acad. Sci. U.S.A.* **96,** 12379–12383
29. Alexander, J. M., Nelson, C. A., van Berkel, V., Lau, E. K., Studts, J. M., Brett, T. J., Speck, S. H., Handel, T. M., Virgin, H. W., and Fremont, D. H. (2002) Structural basis of chemokine sequestration by a herpesvirus decoy receptor. *Cell* **111,** 343–356
30. Derider, M. L., Zhang, L., and Liwang, P. J. (2006) Resonance assignments and secondary structure of vCCI, a 26 kDa CC chemokine inhibitor from rabbitpox virus. *J. Biomol. NMR* **36,** 22
31. Zhang, L., and Liwang, P. J. (2006) Resonance assignments of the 34 kD rabbitpox vCCI:human MIP-1β complex. *J. Biomol. NMR* **36,** 49
32. Zhang, L., Derider, M., McCornack, M. A., Jao, S. C., Isern, N., Ness, T., Moyer, R., and LiWang, P. J. (2006) Solution structure of the complex between poxvirus-encoded CC chemokine inhibitor vCCI and human MIP-1β. *Proc. Natl. Acad. Sci. U.S.A.* **103,** 13985–13990
33. Arnold, P. L., and Fremont, D. H. (2006) Structural determinants of chemokine binding by an Ectromelia virus-encoded decoy receptor. *J. Virol.* **80,** 7439–7449
34. Alexander-Brett, J. M., and Fremont, D. H. (2007) Dual GPCR and GAG mimicry by the M3 chemokine decoy receptor. *J. Exp. Med.* **204,** 3157–3172
35. Bahar, M. W., Kenyon, J. C., Putz, M. M., Abrescia, N. G., Pease, J. E., Wise, E. L., Stuart, D. I., Smith, G. L., and Grimes, J. M. (2008) Structure and function of A41, a vaccinia virus chemokine binding protein. *PLoS Pathog.* **4,** e5
36. Antonets, D. V., Nepomnyashchikh, T. S., and Shchelkunov, S. N. (2010) SECRET domain of variola virus CrmB protein can be a member of poxviral type II chemokine-binding proteins family. *BMC Res. Notes* **3,** 271
37. Dias, J. M., Losberger, C., Déruaz, M., Power, C. A., Proudfoot, A. E., and Shaw, J. P. (2009) Structural basis of chemokine sequestration by a tick chemokine binding protein. The crystal structure of the complex between Evasin-1 and CCL3. *PLoS One* **4,** e8514
38. Seet, B. T., Singh, R., Paavola, C., Lau, E. K., Handel, T. M., and McFadden, G. (2001) Molecular determinants for CC-chemokine recognition by a poxvirus CC-chemokine inhibitor. *Proc. Natl. Acad. Sci. U.S.A.* **98,** 9008–9013
39. Crump, M. P., Rajarathnam, K., Kim, K. S., Clark-Lewis, I., and Sykes, B. D. (1998) Solution structure of eotaxin, a chemokine that selectively recruits eosinophils in allergic inflammation. *J. Biol. Chem.* **273,** 22471–22479
40. Pease, J. E. (2011) Targeting chemokine receptors in allergic disease.

Biochem. J. **434,** 11–24
41. Bisset, L. R., and Schmid-Grendelmeier, P. (2005) Chemokines and their receptors in the pathogenesis of allergic asthma. Progress and perspective. *Curr. Opin. Pulm. Med.* **11,** 35–42
42. Wells, T. N., Power, C. A., Shaw, J. P., and Proudfoot, A. E. (2006) Chemokine blockers. Therapeutics in the making? *Trends Pharmacol. Sci.* **27,** 41–47
43. Dominiguez, C., Boelens, R., and Bonvin, A. M. (2003) HADDOCK. A protein-protein docking approach based on biochemical or biophysical information. *J. Am. Chem. Soc.* **125,** 1731–1737
44. de Vries, S. J., van Dijk, A. D., Krzeminski, M., van Dijk, M., Thureau, A., Hsu, V., Wassenaar, T., and Bonvin, A. M. (2007) HADDOCK *versus* HADDOCK. New features and performance of HADDOCK2.0 on the CAPRI targets. *Proteins* **69,** 726–733
45. Mossessova, E., and Lima, C. D. (2000) Ulp1-SUMO crystal structure and genetic analysis reveal conserved interactions and a regulatory element essential for cell growth in yeast. *Mol. Cell* **5,** 865–876
46. Xue, J., Kuo, N., Schill, M. S., and LiWang, P. J. (2013) A comparison of 5P12-vMIP-II and vMIP-II as HIV-1 entry inhibitors. *Biochem. Physiol.* 10.4172/2168-9652.S2-005
47. Delaglio, F., Grzesiek, S., Vuister, G. W., Zhu, G., Pfeifer, J., and Bax, A. (1995) NMRPipe. A multidimensional spectral processing system based on UNIX pipes. *J. Biomol. NMR* **6,** 277–293
48. Johnson, B. A. (2004) Using NMRView to visualize and analyze the NMR spectra of macromolecules. *Methods Mol. Biol.* **278,** 313–352
49. Goddard, T. D., and Kneller, D. G. Sparky 3. University of California, San Francisco, CA
50. Jung, Y. S., and Zweckstetter, M. (2004) Mars. Robust automatic backbone assignment of proteins. *J. Biomol. NMR* **30,** 11–23
51. Salzmann, M., Wider, G., Pervushin, K., Senn, H., and Wüthrich, K. (1999) TROSY-type triple-resonance Experiments for sequential NMR assignments of large proteins. *J. Am. Chem. Soc.* **121,** 844–848
52. Salzmann, M., Wider, G., Pervushin, K., and Wüthrich, K. (1999) Improved sensitivity and coherence selection for [^{15}N,^{1}H]-TROSY elements in triple resonance experiments. *J. Biomol. NMR* **15,** 181–184
53. Loria, J. P., Rance, M., and Palmer, A. G., 3rd (1999) Transverse-relaxation-optimized (TROSY) gradient-enhanced triple-resonance NMR spectroscopy. *J. Magn. Reson.* **141,** 180–184
54. Tjandra, N., Grzesiek, S., and Bax, A. (1996) Magnetic field dependence of nitrogen-proton J splittings in N-15-enriched human ubiquitin resulting from relaxation interference and residual dipolar coupling. *J. Am. Chem. Soc.* **118,** 6264–6272
55. Garrett, D. S., Seok, Y. J., Peterkofsky, A., Clore, G. M., and Gronenborn, A. M. (1997) Identification by NMR of the binding surface for the histidine-containing phosphocarrier protein HPr on the N-terminal domain of enzyme I of the *Escherichia coli* phosphotransferase system. *Biochemistry* **36,** 4393–4398
56. de Vries, S. J., van Dijk, M., and Bonvin, A. M. (2010) The HADDOCK web server for data-driven biomolecular docking. *Nat. Protoc.* **5,** 883–897
57. Willard, L., Ranjan, A., Zhang, H., Monzavi, H., Boyko, R. F., Sykes, B. D., and Wishart, D. S. (2003) VADAR. A web server for quantitative evaluation of protein structure quality. *Nucleic Acids Res.* **31,** 3316–3319
58. Conlan, L. H., and Dupureur, C. M. (2002) Dissecting the metal ion dependence of DNA binding by PvuII endonuclease. *Biochemistry* **41,** 1335–1342
59. Reid, S. L., Parry, D., Liu, H. H., and Connolly, B. A. (2001) Binding and recognition of GATATC target sequences by the EcoRV restriction endonuclease. A study using fluorescent oligonucleotides and fluorescence polarization. *Biochemistry* **40,** 2484–2494
60. Delaglio, L. K., J. (2004) *DYNAMO. A structure calculation and analysis program*. National Institutes of Health, Bethesda, MD
61. Seet, B. T., and McFadden, G. (2002) Viral chemokine-binding proteins. *J. Leukoc. Biol.* **72,** 24–34
62. Alcami, A., Symons, J. A., Collins, P. D., Williams, T. J., and Smith, G. L. (1998) Blockade of chemokine activity by a soluble chemokine binding protein from vaccinia virus. *J. Immunol.* **160,** 624–633
63. Gabriel, P., Babiarova, K., Zurkova, K., Krystofova, J., Hainz, P., Kutinova, L., and Nemeckova, S. (2012) Chemokine binding protein vCCI attenuates vaccinia virus without affecting the cellular response elicited by immunization with a recombinant vaccinia vector carrying the HPV16 E7 gene. *Viral Immunol.* **25,** 411–422
64. McCornack, M. A., Cassidy, C. K., and LiWang, P. J. (2003) The binding surface and affinity of monomeric and dimeric chemokine MIP-1b for various glycosaminoglycan disaccharides. *J. Biol. Chem.* **278,** 1946–1956
65. Koopmann, W., Ediriwickrema, C., and Krangel, M. S. (1999) Structure and function of the glycosaminoglycan binding site of chemokine macrophage inflammatory protein-1b. *J. Immunol.* **163,** 2120–2127
66. Lalani, A. S., Graham, K., Mossman, K., Rajarathnam, K., Clark-Lewis, I., Kelvin, D., and McFadden, G. (1997) The purified myxoma virus γ interferon receptor homolog M-T7 interacts with the heparin-binding domains of chemokines. *J. Virol.* **71,** 4356–4363
67. Webb, L. M., Smith, V. P., and Alcami, A. (2004) The gammaherpesvirus chemokine binding protein can inhibit the interaction of chemokines with glycosaminoglycans. *FASEB J.* **18,** 571–573
68. Laurence, J. S., Blanpain, C., Burgner, J. W., Parmentier, M., and LiWang, P. J. (2000) The CC chemokine MIP-1b can function as a monomer and depends on Phe^{13} for receptor binding. *Biochemistry* **39,** 3401–3409
69. Nardese, V., Longhi, R., Polo, S., Sironi, F., Arcelloni, C., Paroni, R., DeSantis, C., Sarmientos, P., Rizzi, M., Bolognesi, M., Pavone, V., and Lusso, P. (2001) Structural determinants of CCR5 recognition and HIV-1 blockade in RANTES. *Nat. Struct. Biol.* **8,** 611–615
70. Hemmerich, S., Paavola, C., Bloom, A., Bhakta, S., Freedman, R., Grunberger, D., Krstenansky, J., Lee, S., McCarley, D., Mulkins, M., Wong, B., Pease, J., Mizoue, L., Mirzadegan, T., Polsky, I., Thompson, K., Handel, T. M., and Jarnagin, K. (1999) Identification of residues in the monocyte chemotactic protein-1 that contact the MCP-1 receptor, CCR2. *Biochemistry* **38,** 13013–13025
71. Salanga, C. L., and Handel, T. M. (2011) Chemokine oligomerization and interactions with receptors and glycosaminoglycans. The role of structural dynamics in function. *Exp. Cell Res.* **317,** 590–601